American Mineralogist, Volume 79, pages 622–632, 1994

X-ray absorption spectroscopy of silicon dioxide (SiO_2) polymorphs: The structural characterization of opal

Dien Li, G. M. Bancroft, M. Kasrai
Department of Chemistry, University of Western Ontario, London, Ontario N6A 5B7, Canada
M. E. Fleet, R. A. Secco
Department of Earth Sciences, University of Western Ontario, London, Ontario N6A 5B7, Canada
X. H. Feng, K. H. Tan, B. X. Yang*
Canadian Synchrotron Radiation Facility, Synchrotron Radiation Center,
University of Wisconsin, Madison, Wisconsin 53589, U.S.A.

Abstract

Si*K*- and Si*L*-edge X-ray absorption spectra obtained using synchrotron radiation are reported for 6:3-coordinated stishovite and 4:2-coordinated α quartz, α cristobalite, coesite, amorphous silica (a-SiO_2), and opal. The Si*K* and Si*L* near-edge features are interpreted on the basis of a qualitative MO model of SiO_4^{4-} and SCF-Xα calculation of model molecules. Some edge features are attributed to the multiple scattering effect of the more distant shell atoms in the crystal structure. The *K*- and *L*-edge features reflect the maximum densities of unoccupied Si 3s, 3p, and 3d states in the conduction band and are qualitatively in agreement with calculated densities of states. Comparison of Si*K*- and Si*L*-edge XANES demonstrates the bond mixing of Si 3p and 3s orbitals and of Si 3p and 3d orbitals. Also, for 4:2-coordinated silica, the transition of Si 2p electrons to the t_2 state of high Si 3p character becomes dipole allowed. For stishovite and coesite, states dominated by Si 3s apparently have a large amount of Si 3p orbital character, probably because of pressure-induced mixing of Si 3s and 3p orbitals. The Si*K*- and Si*L*-edge shifts are systematically related to the coordination number of Si atoms, Si-O bond length, Si-Si distance, Si-O-Si angle, Si-O bond valence, and Si NMR chemical shift of SiO_2 polymorphs. The Si*K*- and Si*L*-edge XANES indicate that the local structure of two opals investigated is a mixture of a-SiO_2 and α cristobalite structural units, and the relative proportions of the two structural components are semiquantitatively determined. EXAFS structure parameters (bond distances, coordination number, and Debye-Waller factor) of quartz and stishovite are obtained and shown to be in good agreement with the X-ray structures. Si in sixfold and fourfold coordination can be distinguished unambiguously from Si*K*- and Si*L*-edge XANES features and Si*K*-edge EXAFS analysis. These results are very useful for characterizing the structure and bonding of the mantle silicates and silicate glasses.

Introduction

Extensive studies on phase transformations of Mg- and Fe-bearing silicates at high temperature and high pressure have been conducted to understand the mineralogical and petrological relations and seismological discontinuities of the Earth's mantle. The phase transformations in $MgSiO_3$ and Mg_2SiO_4, two of the most important silicate compositions, have been established as follows (Liu, 1975): with increasing pressure, the sequence of transformations is enstatite ($MgSiO_3$) to β spinel and stishovite, to γ spinel and stishovite, to ilmenite, and finally to perovskite phases, whereas forsterite (Mg_2SiO_4) transforms to β spinel, to γ spinel, and finally to perovskite and periclase. The densification of silicates at high pressure is caused by more efficient packing of anions or an increase in the coordination number of cations (or both).

There are many polymorphic modifications of silicon dioxide (SiO_2) at high temperature and high pressure, including 4:2-coordinated structures (α quartz, cristobalite, tridymite, and coesite) and a 6:3-coordinated structure (stishovite). Stishovite was initially synthesized at high pressure above 100 kbar (Stishov and Popova, 1961) and subsequently discovered in an impact breccia from Meteorite Crater, Arizona (Chao et al., 1962). Stishovite has a rutile-type structure (Sinclair and Ringwood, 1978). The detailed crystal chemistry of stishovite was described by Hill et al. (1983) and Ross et al. (1990). The electronic structures of α quartz, β cristobalite, and stishovite have been calculated using various approaches. The calculated valence band structures were used to interpret reasonably

* Present address: Advanced Photon Sources, Argonne National Laboratory, Argonne, Illinois 60439-4814, U.S.A.

0003–004X/94/0708–0622$02.00

the experimental photoelectron spectra (XPS and UPS) and X-ray emission spectra (XES). The recent references on these calculations have been listed in Li et al. (1993). Wiech and Kurmaev (1985) also studied the electronic structure of crystalline and vitreous SiO_2 using Si*K* XES.

The valence band (VB) structure and bonding of α quartz, β cristobalite, and stishovite are well understood from experimental XPS and XES, as well as from theoretical calculations. X-ray absorption near-edge structure (XANES) can provide important information on the unoccupied electronic states of solids. The Si$L_{2,3}$-edge XANES of α quartz was first reported by Brown et al. (1977). The Si*K*- and Si$L_{2,3}$-edge XES and X-ray absorption spectra (XAS) of stishovite and α quartz have been studied comparatively (Iguchi, 1977; Brytov et al., 1979). Recently, Davoli et al. (1992) also studied the Si*K*-edge and O*K*-edge XANES of densified a-SiO_2 at high pressure. However, the assignments for the XANES spectra of both α quartz and stishovite were in conflict, and the conduction band (CB) structure and unoccupied densities of states of SiO_2 are not fully understood, mainly because of theoretical and experimental limitations. We recently reported the high-resolution Si*K*- and Si*L*-edge XANES of α quartz and 6:3-coordinated stishovite using synchrotron radiation (Li et al., 1993).

In this paper, we present high-resolution Si*K*- and Si*L*-edge XANES and Si*K*-edge EXAFS of 6:3-coordinated stishovite and 4:2-coordinated α quartz, α cristobalite, coesite, amorphous SiO_2, and opals and use the spectra to infer the unoccupied electronic states of these forms of silica (SiO_2). In addition, we explore the relation of the XANES spectra to the crystal structures of SiO_2 polymorphs and discuss important new applications of XANES and EXAFS to study amorphous silicate materials.

Experimental methods

Natural and synthetic stishovite samples were provided by Lin-gun Liu, Australian National University. The natural stishovite was separated from sandstone of the Meteorite Crater, Arizona, by German researchers (Liu, 1993 personal communication). The synthetic stishovite was obtained by allowing coesite and graphite to react at 120 kbar. Natural single-crystal α quartz and the two opal samples were from the mineral collection in the Department of Earth Sciences, University of Western Ontario (UWO). Two cristobalite samples were synthesized at room pressure and 1600 °C, and the coesite sample was synthesized at 1000 °C and 50 kbar using the 1000-t cubic-anvil press at UWO. All samples were checked by X-ray powder diffraction (XRD) before X-ray absorption spectra (XAS) measurements were obtained. Both samples of opal were highly disordered and nearly amorphous. Opal no. 1232 was a precious opal from Queensland, Australia, and has an XRD pattern similar to sample H (Jones and Segnit, 1971). Opal no. 800 was from Virgin, Nevada, and had an XRD pattern intermediate between that of samples G and F (Jones and Segnit, 1971).

The *K*-edge XAS were measured using a double-crystal monochromator (DCM) with synchrotron radiation at the chamber pressure of 10^{-6} torr. The DCM employs InSb (111) as the monochromator crystals. The spectra of the fine powder samples were recorded using both total electron yield (TEY) and fluorescence modes. The energy resolution for the DCM is about 0.8 eV at 1840 eV so that the line width for the Si*K*-edge of α quartz is as small as 1.7 eV. The *K*-edge XANES spectra were obtained at an interval of 0.2 eV, with 2 s for each data point; the EXAFS data were collected at an interval of 0.3–4 eV, with 2–5 s per data point from 1900 to 2800 eV, so that the data have the same interval in **k** space after Fourier transform. The *L*-edge XANES were collected at the chamber pressure of 10^{-8} torr with a Grasshopper monochromator by TEY, which has an energy resolution of about 0.1 eV at 100 eV. The DCM and Grasshopper beam lines are affiliated with the Canadian Synchrotron Radiation Facility (CSRF) and accommodated on the Aladdin storage ring operating at either 800 MeV, with current from 50 to 180 mA, or 1 GeV, with current from 40 to 80 mA, in the Synchrotron Radiation Center (SRC), University of Wisconsin. The designs and performances were described for the DCM by Yang et al. (1992) and for the Grasshopper beam line by Bancroft (1992).

Results and discussion

Interpretation of XANES spectra

Figure 1 shows the Si*K*- and Si$L_{2,3}$-edge XANES of α quartz and stishovite, along with the calculated unoccupied density of state (Nucho and Madhukar, 1980; Li and Ching, 1985). There are no significant differences between our TEY and fluorescence spectra, but all present observations and interpretation are based on the TEY spectra. The $L_{2,3}$-edge spectra are aligned using the XPS Si 2p binding energy (BE) of α quartz at 103.4 eV (Wagner et al., 1982), and the Si*K*-edge spectra are correlated with the Si$L_{2,3}$-edge spectra by taking the Si$K\alpha_1$ X-ray emission line of α quartz at 1740.0 eV. The peak positions are summarized in Table 1, in which ΔE is the difference between the XANES resonance and the corresponding Si 1s or 2p BE of α quartz. The ΔE value for the corresponding peaks A–G in the *L*- and *K*-edge spectra of both minerals are very similar, although the relative intensities differ considerably. The slight ΔE differences of the corresponding *L*- and *K*-edge spectra features are probably attributable to differences in *L* and *K* core-hole relaxation. The calculated density of state features also correspond reasonably well in most cases with the *L*- and *K*-edge features (Fig. 1), although, again, relative intensities differ considerably.

XANES features involve complicated processes and are not fully understood theoretically. For molecules, the inner-potential barrier model (Dehmer, 1972; Hudson et al., 1993) and multiple scattering Xα calculation (Tse et al., 1989) have been used successfully to interpret the majority of features in the XANES spectra of many molecules. For semiconductors and insulators, calculated

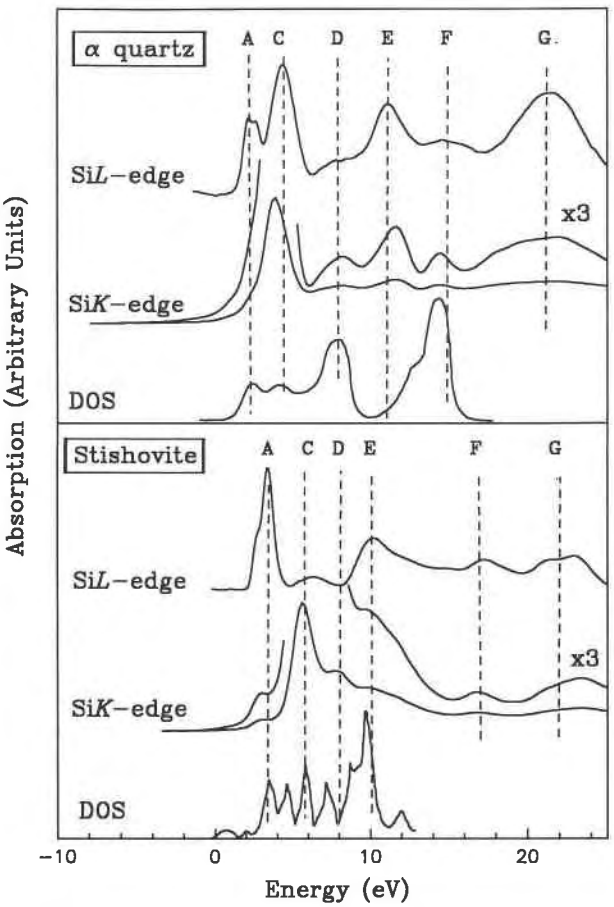

Fig. 1. High-resolution SiK- and Si$L_{2,3}$-edge XANES of 4:2-coordinated α quartz and 6:3-coordinated stishovite. The calculated unoccupied densities of states are cited from Nucho and Madhukar (1980) for α quartz and from Li and Ching (1985) for stishovite. The Si 2p XPS BE of α quartz is 103.4 eV (Wagner et al., 1982), and the Si 1s BE is calculated by the sum of the Si 2p XPS BE and Si$K\alpha_1$ XES at 1740.0 eV. The SiK- and Si$L_{2,3}$-edge XANES spectra are aligned to zero using the Si 1s and 2p BE, respectively.

densities of states within the energy band theory (Brown et al., 1977), the multiple scattering approach (Natoli and Benfatto, 1986), the one-electron approximation molecular orbital diagram (Iguchi, 1977; Brytov et al., 1979; Kisiel et al., 1989), and a quasi-molecular method (Filatova et al., 1985) have been proposed to interpret the near-edge features. Lately, we have successfully interpreted qualitatively the SiK- and SiL-edge features of 4:2-coordinated α quartz on the basis of the SiK- and SiL-edge XANES, as well as SCF-Xα calculations of molecular model compounds (Sutherland et al., 1993). Therefore, for semiconducting and insulating solids, the strong near-edge features, like the strong line structures in the XAS of molecules, correspond to the transitions of inner-shell electrons to unoccupied states in the CB. If one assumes L-S coupling in absorber atoms, these transitions are also governed by the dipole selection rules, $\Delta L = \pm 1$, $\Delta S = 0$, and $\Delta J = \pm 1$.

The SiL-edge XANES (Iguchi, 1977) and both SiK- and SiL-edge XANES (Brytov et al., 1979) of α quartz and stishovite were reported and interpreted on the basis of the MO calculations of SiO_4^{4-} and SiO_8^{8-} clusters. Recently, Azizan et al. (1987) used the MO calculation of the SiO_4^{4-}-cluster to interpret the direct and inverse photoemission spectra of crystalline and amorphous SiO_2 and to study the electronic structures of these materials. In the ground state of the SiO_4^{4-} moleculelike cluster having T_d point symmetry, the s orbitals of the Si atom transform to an a_1 representation, the p orbitals transform to a t_2 representation, and the d orbitals split into triply degenerate t_2 and doubly degenerate e representations. The transitions of Si 1s electrons to these unoccupied states are allowed by electric dipole selections (Iguchi, 1977; Hansen et al., 1992).

For 4:2-coordinated α quartz, the Si XANES spectra are characteristic of a tetrahedral SiO_4 cluster. Indeed, the main peaks, A, C, E, and G, in both K- and L-edge XANES are aligned well and can be assigned generally from the gas phase spectra of the tetrahedral analogues $Si(OCH_3)_4$ (Sutherland et al., 1993), SiH_4 (Friedrich et al., 1979), and SiF_4 (Ferrett et al., 1988). Based on the molecular orbital approach mentioned above (Tossell, 1975a; Iguchi, 1977; Azizan et al., 1987), peak A in the L-edge XANES corresponds to a transition of Si 2p electrons to the antibonding a_1 state (Si 3s-like state). The splitting of this peak by about 0.6 eV is attributed to the spin-orbital interaction of Si 2p orbitals. O'Brien et al. (1991) determined the CB minimum of α quartz at 106.73 eV on the basis of the Si$L_{2,3}$ XES at 97.3 eV and the known optical band gap of 9.1 eV (Ravindra and Narayan, 1987). Therefore, peak A is also called a core exciton below the CB minimum of α quartz (Bianconi, 1979). Peak A in the K-edge XANES is weak because the transition of Si 1s → Si 3s-like state is dipole forbidden. Peak C in the SiK-edge spectrum is attributed to the dipole-allowed transition of Si 1s electrons to the antibonding t_2 state of majority Si 3p character, and peak C in the L-edge spectra to the transition of Si 2p electrons to the t_2 state. The high intensity of peak C in the L-edge spectrum shows that even though the peak corresponds to a Si 2p → p-like transition, a $t_2 \rightarrow t_2$ transition is, in fact, dipole allowed (Iguchi, 1977; Hansen et al., 1992). This is also consistent with the acentric tetrahedral symmetry and the strong hybridization of the Si 3s, 3d, and 3p orbitals in α quartz. Peaks E and G in the L-edge XANES are assigned to the empty Si 3d states (Liu et al., 1992), also called shape resonances (Bianconi, 1979). In the T_d crystal field, the 3d orbitals are split into e and t_2 states, and the e states are favored in energy over t_2. Peak E is assigned to transitions to the e states, and peak G to the t_2 states. The Si 3d states in α quartz also have contributions from Si p electron states, which are responsible for peaks E and G in the SiK-edge XANES of α quartz.

Peaks D and F in both K- and L-edge spectra of α quartz correspond with peaks in the density of state. However, these two peaks are not present in both SiK- and SiL-edge XANES of a-SiO_2, the theoretical calcula-

TABLE 1. Si*K*- and Si$L_{2,3}$-edge XANES of SiO_2 polymorphs

	K-edge (eV)			$L_{2,3}$-edge (eV)		
	Peaks	ΔE*	Assignments**	Peaks	ΔE*	Assignments**
			α quartz			
A	1844.9	1.5	Si 1s → a_1 (Si 3s-3p)	105.4	2.0	Si $2p_{3/2}$ → a_1 (Si 3s-3p)
				106.0	2.6	Si $2p_{1/2}$ → a_1 (Si 3s-3p)
C	1846.8	3.4	Si 1s → t_2 (Si 3p-3s)	107.8	4.4	Si 2p → t_2 (Si 3p-3s)
D	1850.7	7.3	multiple scattering	111.3	7.9	multiple scattering
E	1854.5	12.1	Si 1s → e (Si 3d-3p)	114.5	11.1	Si 2p → e (Si 3d-3p)
F	1857.4	14.0	multiple scattering	118.5	15.1	multiple scattering
G	1864.3	20.9	Si 1s → t_2 (Si 3d-3p)	125.0	21.6	Si 2p → t_2 (Si 3d-3p)
			Cristobalite			
A	1844.9	1.5	Si 1s → a_1 (Si 3s-3p)	105.6	2.2	Si $2p_{3/2}$ → a_1 (Si 3s-3p)
				106.2	2.8	Si $2p_{1/2}$ → a_1 (Si 3s-3p)
C	1846.74	3.3	Si 1s → t_2 (Si 3p-3s)	108.0	4.6	Si 2p → t_2 (Si 3p-3s)
D	1849.9	6.5	multiple scattering	111.3	8.3	multiple scattering
E	1852.6	9.2	Si 1s → e (Si 3d-3p)	114.2	10.8	Si 2p → e (Si 3d-3p)
F	1856.5	13.1	multiple scattering	115.9	12.5	multiple scattering
G	1863.6	20.2	Si 1s → t_2 (Si 3d-3p)	127.8	21.2	Si 2p → t_2 (Si 3d-3p)
			Coesite			
A	1843.6	0.2	Si 1s → a_1 (Si 3s-3p)	105.9	2.5	Si $2p_{3/2}$ → a_1 (Si 3s-3p)
				106.5	3.1	Si $2p_{1/2}$ → a_1 (Si 3s-3p)
C	1846.8	3.4	Si 1s → t_2 (Si 3p-3s)	107.8	4.4	Si 2p → t_2 (Si 3p-3s)
D	1851.1	7.7	multiple scattering	111.3	7.9	multiple scattering
E	1855.0	11.6	Si 1s → e (Si 3d-3p)	114.3	10.9	Si 2p → e (Si 3d-3p)
F	1858.4	15.0	multiple scattering	116.5	13.1	multiple scattering
G	1864.0	20.6	Si 1s → t_2 (Si 3d-3p)	125.9	22.5	Si 2p → t_2 (Si 3d-3p)
			a-SiO_2			
A	1844.9	1.5	Si 1s → a_1 (Si 3s-3p)	104.8	1.4	Si $2p_{3/2}$ → a_1 (Si 3s-3p)
				105.4	2.2	Si $2p_{1/2}$ → a_1 (Si 3s-3p)
C	1846.9	3.5	Si 1s → t_2 (Si 3p-3s)	107.7	4.3	Si 2p → t_2 (Si 3p-3s)
E	1853.4	10.0	Si 1s → e (Si 3d-3p)	114.8	11.3	Si 2p → e (Si 3d-3p)
G	1863.8	20.4	Si 1s → t_2 (Si 3d-3p)	131.1	27.3	Si 2p → t_2 (Si 3d-3p)
			Opal			
A	1844.9	1.5	Si 1s → a_1 (Si 3s-3p)	105.5	2.1	Si $2p_{3/2}$ → a_1 (Si 3s-3p)
				106.2	2.8	Si $2p_{1/2}$ → a_1 (Si 3s-3p)
C	1846.8	3.4	Si 1s → t_2 (Si 3p-3s)	108.1	4.7	Si 2p → t_2 (Si 3p-3s)
E	1852.7	9.3	Si 1s → e (Si 3d-3p)	115.1	11.7	Si 2p → e (Si 3d-3p)
G	1863.6	20.2	Si 1s → t_2 (Si 3d-3p)	130.4	27.0	Si 2p → t_2 (Si 3d-3p)
			Stishovite			
A	1846.3	2.9	Si 1s → a_{1g} (Si 3s-3p)	106.0	2.6	Si $2p_{3/2}$ → a_{1g} (Si 3s-3p)
				106.8	3.4	Si $2p_{1/2}$ → a_{1g} (Si 3s-3p)
C	1849.0	5.6	Si 1s → t_{1u} (Si 3p-3s)	109.8	6.4	Si 2p → t_{1u} (Si 3p-3s)
D	1851.3	7.9	multiple scattering			
E	1853.4	10.0	Si 1s → t_{2g} (Si 3d-3p)	113.6	10.2	Si 2p → t_{2g} (Si 3d-3p)
F	1860.2	16.8	multiple scattering	120.7	17.3	multiple scattering
G	1866.4	23.0	Si 1s → e_g (Si 3d-3p)	126.4	23.0	Si 2p → e_g (Si 3d-3p)

* The XPS Si 2p BE of α quartz is 103.4 eV, and the Si$K\alpha_1$ X-ray emission energy is 1740.0 eV, so that the Si 1s BE is calculated to be 1843.4 eV. The ΔE is the energy difference between the resonances and the Si 1s BE for the Si*K*-edge XANES and between the resonances and the Si 2p BE for the Si$L_{2,3}$-edge XANES.

** The majority character of the conduction band states is given first.

tions of gaseous $Si(OCH_3)_4$ and $Si(CH_3)_4$ (Sutherland et al., 1993), and the Si*L*-edge XANES of SiH_4 (Friedrich et al., 1979) and SiF_4 (Ferrett et al., 1988). On the other hand, McComb et al. (1992) have done multiple-scattering calculations (MS) for zircon ($ZrSiO_4$). The results indicated that with increasing the size of the cluster, although s- and d-like final states are essentially localized in the first coordination shell, the p-like DOS is modified by outer shells. When the MS calculation was made for the SiO_4^{4-}cluster, the calculated spectrum is similar to that of a-SiO_2. When up to seven shells are included in the MS calculation, the Si*K*-edge electron energy loss near-edge structure (ELNES) is reproduced. The peaks, because of the MS effect, which is absent in the SiO_4^{4-} spectrum, correspond well to peaks D and F in our Si*K*-edge XANES spectrum of α quartz. From this argument, peaks D and F are probably related to the extended energy band structure or the MS of the more distant shell atoms in the crystal structure. Davoli et al. (1992) reported the Si*K*-edge spectra of densified vitreous silica; however, their spectra had lower signal to noise ratios, and their MS calculations are not in their experimental results or their conclusions. More recently, Bart et al. (1993) interpreted peaks D, E, F, and G in the Si*K*-edge spectrum of α quartz as the MS from the more distant atoms using Natoli's model (Natoli, 1984), but they did not even include the first Si-O shell in the ΔE vs. $1/R^2$ correlation. Actually, we tried to use this model, but it does not work for our spectra of α quartz and many other silicate minerals.

The very different spectra for 6:3-coordinated stisho-

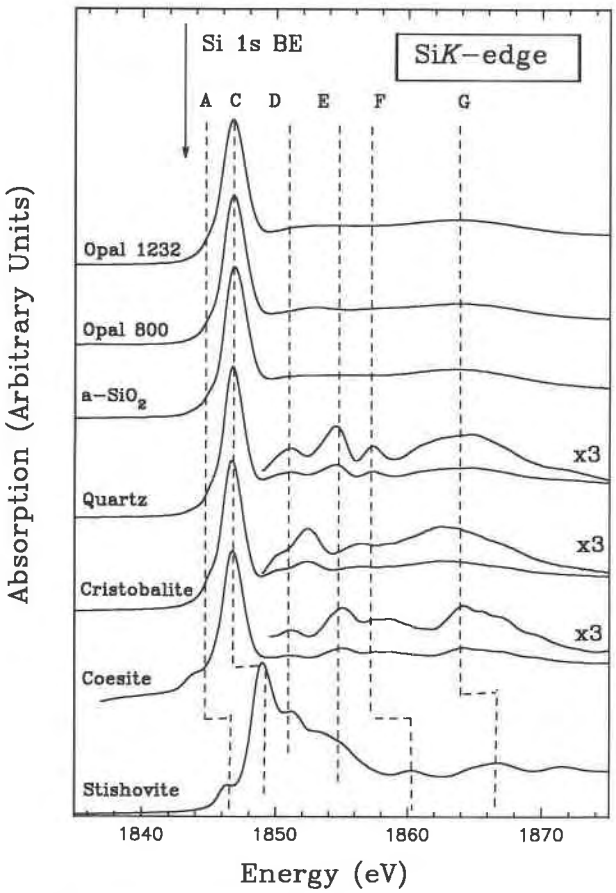

Fig. 2. Si*K*-edge XANES spectra of 6:3-coordinated stishovite and 4:2-coordinated α quartz, α cristobalite, coesite, amorphous SiO_2, and opal. The Si 1s BE is indicated by an arrow, and the peaks are labeled as in Fig. 1. The features above the edge (peak C) have been enhanced.

vite can be interpreted qualitatively with the help of the Si*K*- and Si*L*-edge spectra of SiF_6 (Ferrett et al., 1986; Hudson et al., 1993) and the MO calculation of the SiO_6^{8-} cluster (Tossell, 1975b; Iguchi, 1977). In octahedral symmetry, the s state transforms to an a_{1g} representation, the p state transforms to a t_{1u} representation, and the d state is split into t_{2g} and e_g orbitals. Therefore, peak A in the *L*-edge spectrum is due to the transition of Si 2p electrons to the antibonding a_{1g} orbital (Si 3s-like state). The splitting of peak A is apparently larger than the Si 2p spin-orbit splitting of 0.6 eV, but this splitting must be mainly due to the Si 2p spin-orbit interaction. Peak A in the *K*-edge spectrum is relatively weak because the transition of Si 1s → 3s is not dipole allowed. Peak C is attributed to the transition of Si 1s electrons to the antibonding t_{1u} orbital (Si 3p-like state). This transition is not formally allowed in the *L*-edge spectrum, and so peak C is very weak in the *L*-edge spectrum, as in the corresponding spectrum of SF_6 (Hudson et al., 1993). In addition, the hybridization of Si 3s, 3d, and Si 3p orbitals in stishovite is much weaker than that in α quartz, because of the octahedral crystal field in stishovite. Peaks E and G in the *L*-edge spectrum can be assigned readily to the d-like shape resonance of t_{2g} and e_g character, respectively. The energy separation of the two Si 3d bands in stishovite is larger than in α quartz, as required for the present assignments, but it does not obey the rule $\Delta_{tet} = -4/9\Delta_{oct}$ (Liu et al., 1992). The empty Si 3d bands are also mixed with some Si p-like states, which are responsible for the weak peaks E and G in the *K*-edge spectrum of stishovite. The origins of peak D in the *K*-edge XANES and peak F in the *K*- and *L*-edge spectrum of stishovite may be related also to the extended energy band structure or MS effects, as discussed for α quartz.

The qualitative assignments of the near Si*K*- and Si*L*-edge spectra of α quartz and stishovite are summarized in Table 1. These assignments are reasonably consistent and also in reasonable agreement with calculated unoccupied density of state (see Fig. 1). Unfortunately, the density of state calculations gave neither the s, p, or d character of these unoccupied states nor the probability of transition to these states (Nucho and Madhukar, 1980; Li and Ching, 1985), and it is not possible to relate the experimental and theoretical intensities even semiqualitatively. We can, however, give a qualitative and reasonable assignment that gives satisfactory relative intensities.

XANES spectra and crystal chemistry

Figure 2 shows the Si*K*-edge XANES spectra of cristobalite, coesite, a-SiO_2, and opals, as well as α quartz and stishovite, in which the Si 1s BE for α quartz is indicated by an arrow at the top left. The Si*K*-edge spectrum of a-SiO_2 is in agreement with the results of Davoli et al. (1992). The peak positions and the assignments are also summarized in Table 1. It is immediately apparent that the XANES spectrum of the 6:3-coordinated stishovite is very different from those of 4:2-coordinated α quartz, cristobalite, and coesite. In 4:2-coordinated SiO_2, the strongest peak, C, at about 1846.8 eV, characterizes the $^{[4]}$Si with O in the Si*K*-edge XANES, and peak A, due to the dipole-forbidden transition of Si 1s → Si 3s, is very weak. However, peak C in the stishovite *K*-edge spectrum is shifted by about 2.2 eV to higher energy compared with peak C in 4:2-coordinated SiO_2, and peak A is significantly intensified, even though the transition of Si 1s → Si 3s is also dipole forbidden in the octahedral field. Peaks F and G also shift to higher energy (Fig. 2). Therefore, on a simple fingerprint basis, it is apparent that Si*K*-edge XANES spectra should be very useful for distinguishing $^{[4]}$Si and $^{[6]}$Si in silicate minerals and glasses.

For 4:2-coordinated cristobalite and coesite, the general spectral profiles are similar to that of α quartz. The four main peaks, A, C, E, and G, are assigned to the transitions of Si 1s electrons to a_1 (Si 3s-like state), t_2 (Si 3p-like state), e, and t_2 (Si 3d-like state) states in tetrahedral symmetry. However, we also can observe some apparent changes in the Si*K*-edge spectra of these 4:2-coordinated SiO_2. First, peak A, because of a dipole-for-

bidden Si 1s → 3s-like transition, is expected to be weak in the *K*-edge spectra, as observed for most 4:2-coordinated SiO_2 materials. However, for coesite, peak A is significantly more intense and shifts toward lower energy. The energy separation between peaks A and C for coesite is about 3.2 eV, similar to that for stishovite. The relative intensity of peak A for coesite is much greater than that for α quartz and cristobalite but smaller than that for stishovite. This indicates that the Si 3s state below the CB minimum is mixed with more of the Si 3p state in the high-pressure structures. Second, peaks E and G in the cristobalite spectrum shift to lower energy, but the energy separation for these two peaks remains similar to that for α quartz and coesite. Peaks D and F, because of the MS effect, also shift to lower energy and become weak compared with the corresponding peaks for α quartz and coesite. These apparent differences in the postedge region of α cristobalite from those of α quartz and coesite must be related to the crystal structures.

Figure 3 shows the Si*L*-edge XANES of SiO_2 polymorphs, a-SiO_2 and opals, and the Si 2p BE for α quartz is also indicated by an arrow. The peaks are labeled as in Figure 1. The basic spectral features for α quartz, cristobalite, and coesite are qualitatively similar to each other but differ from those of stishovite. The Si*L*-edge (peak A) for stishovite also shifts to higher energy by about 1 eV compared with the $^{[4]}SiO_2$ materials. The Si*L*-edge spectra can also be used as a structural fingerprint to distinguish $^{[4]}$Si and $^{[6]}$Si in silicate minerals and glasses. For the 4:2-coordinated SiO_2 materials, the strong peak, C, at 107.9 ± 0.1 eV, characterizes the $^{[4]}$Si atoms in the Si*L*-edge XANES. However, peak A, an exciton below the CB minimum, appears to shift toward higher energy in the sequence from α quartz to cristobalite to coesite. This slight shift for peak A is related to the local structure of the Si atoms and is also qualitatively in agreement with various crystal chemical parameters, e.g., Si-O bond length, Si-Si distance, Si-O bond valence, and MAS NMR chemical shifts (also see Table 2). As we noted above, comparison with the Si*L*-edge spectrum of gaseous $Si(OCH_3)_4$ (Sutherland et al., 1993), SiH_4 (Friedrich et al., 1979), and SiF_4 (Ferrett et al., 1988) suggests that the Si*L*-edge absorption spectra of various SiO_2 materials are dominated by the $^{[4]}SiO_4^{4-}$ cluster. Hence, the presently resolved differences among the spectra of α quartz, α cristobalite, and coesite, and also among the spectra between crystalline and amorphous SiO_2 materials, likely represent contributions from beyond the first shell of Si; in other words, the extra features reflect the medium-range structure of α quartz, α cristobalite, and coesite.

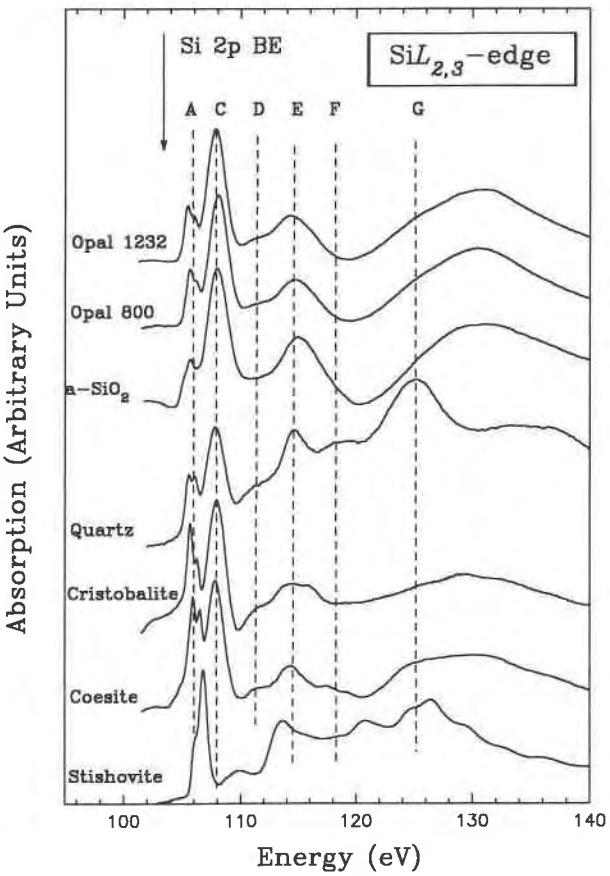

Fig. 3. Si*L*-edge XANES spectra of 6:3-coordinated stishovite and 4:2-coordinated α quartz, α cristobalite, coesite, amorphous SiO_2, and opal. The Si 2b BE is indicated by an arrow, and the peaks are labeled as in Fig. 1.

Table 2. Si*K*- and Si$L_{2,3}$-edge XANES and the crystal chemistry of SiO_2 polymorphs

	α quartz	α cristobalite	Coesite	Stishovite
ΔE for peak C in *K*-edge* (eV)	3.4	3.3	3.4	5.6
ΔE for peak A in $L_{2,3}$-edge* (eV)	2.3	2.5	2.8	3.0
Si:O coordination number	4:2	4:2	4:2	6:3
Si-O (Å)	1.61	1.605	1.61**	1.76 (× 2) 1.81 (× 4)
Si-Si (Å)	3.06	3.07	3.09**	3.24
Si-O-Si (°)	144.0	146.8	150.8**	130.7
Si-O bond valence (*s*)	4.23	4.29	4.22	3.82
MAS NMR δ (ppm)	−107.1	−108.5	−110.0**	−191.1

* The ΔE is the difference between the energy for peak C and Si 1s BE for Si*K*-edge XANES and between the energy for peak A and Si 2p BE for Si$L_{2,3}$-edge XANES.

** There are two Si sites in coesite, but the XANES has no capability to distinguish them. These data are the average of two different Si sites.

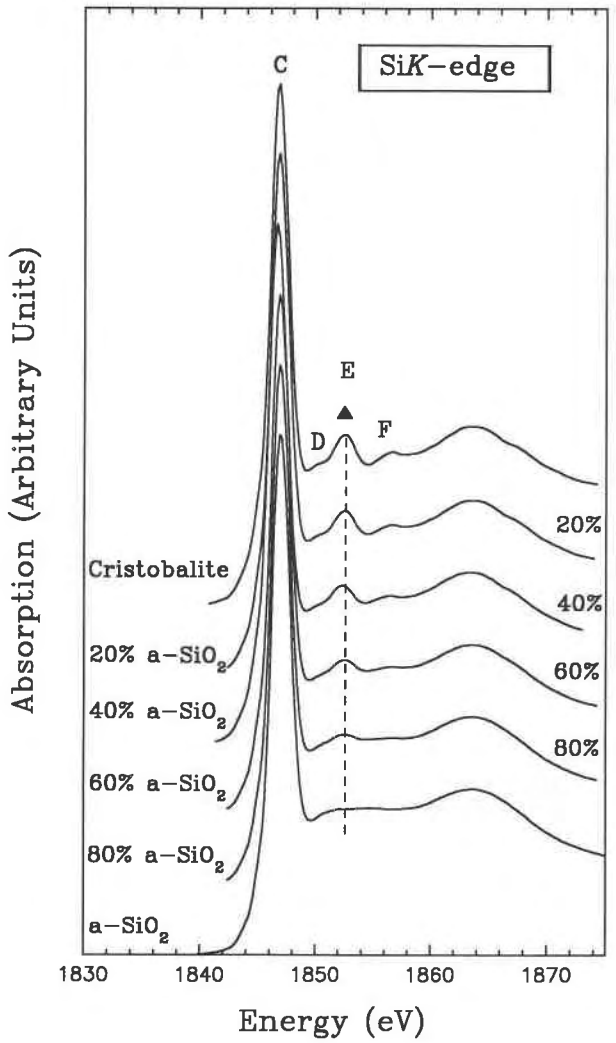

Fig. 4. SiK-edge XANES spectra of cristobalite and a-SiO_2, together with the composite spectra for different proportions of cristobalite and a-SiO_2. The spectra of cristobalite and a-SiO_2 were collected at similar experimental conditions and normalized by I/I_0. A linear background has been removed, and peak C is normalized to the same height in all the spectra. Peak E becomes more intense, as marked by a solid triangle, with an increase in the proportion of cristobalite.

For a-SiO_2, the four main peaks, A, C, E, and F, characterizing [4]Si, are also present in both SiK- and SiL-edge XANES; even peak E in the L-edge spectrum becomes broader and weaker. This confirms that the local structure of a-SiO_2 has tetrahedral symmetry, as in the crystalline 4:2-coordinated modifications. This is, of course, well known from the early diffraction study of a-SiO_2 by Wong and Angell (1976). On the other hand, peaks D and F are absent from both SiK- and L-edge XANES. This confirms the assignments of peaks D and F to the MS effect related to intermediate range structure because the MS effect from the more distant shell atoms are strongly quenched by the structural disorder.

The energy position (ΔE) for peak C in the K-edge XANES and peak A in the L-edge XANES and some crystal chemical parameters of the 4:2-coordinated SiO_2 materials and 6:3-coordinated stishovite are summarized in Table 2. In this table, ΔE is defined as in Table 1, and the bond valence, s, is calculated according to the formula $s = \exp[-(R - R_0)/B]$, where R is the bond length, and R_0 and B are fitted constants for Si-O bonds (Brown, 1981). The shift in the SiK-edge toward higher energy in stishovite is caused by the different effective charge on the Si atoms, which is related to a change of coordination number of Si, from 4 in all 4:2-coordinated SiO_2 materials to 6 in stishovite. This is also in agreement with the Si $K\alpha$ X-ray emission shift and MO calculation (Okura et al., 1990). However, the shift in the SiK-edge XANES is much more significant than that in Si$K\alpha$ X-ray emission. Therefore, the SiK-edge XANES is a more sensitive fingerprint for determining the coordination of Si in silicate minerals and glasses. The SiK-edge shift toward higher energy is also related to variations in crystal chemical parameters of stishovite and the other SiO_2 polymorphs (see Table 2): with an increase in Si-O bond length, Si-Si bond distance, and negative Si MAS NMR chemical shift (Smith and Blackwell, 1983), a decrease in the Si-O-Si bond angle, and a reduction in Si-O bond valence from the 4:2-coordinated SiO_2 polymorphs to stishovite, the SiK-edge shifts toward higher energy.

Structural characterization of opal

Opal is a compact form of natural hydous silica ($SiO_2 \cdot nH_2O$) and has been classified by Jones and Segnit according to the nature of its XRD pattern (Jones and Segnit, 1971). Amorphous opal has been further classified as glass-like network structure opal and gel-like structure opal by Langer and Flörke (1974) on the basis of XRD, chemical, thermoanalytic, and IR spectroscopic studies. Adams et al. (1991) reported that chemical shifts from MAS NMR spectra do not distinguish various types of opal, but the ^{29}Si line widths decrease with an increase in structural order.

The SiK- and SiL-edge XANES spectra of two opal samples, nos. 1232 and 800, are compared with the spectra of the other crystalline SiO_2 polymorphs in Figures 2 and 3, respectively. The SiK-edge spectra of the opal samples are similar to that of a-SiO_2, but we can see some weak features due to long-range ordered structure, particularly for opal no. 800. For example, peak E in the K-edge spectrum of opal no. 800 shifts toward lower energy, as in the spectrum of cristobalite rather than that of α quartz. The SiL-edge spectra of the opals demonstrate that the two opals are essentially similar to a-SiO_2 but also have some spectral features of crystalline cristobalite. For instance, peak A is split, and peak D becomes more significant, as in the cristobalite spectrum. In summary, the two opals essentially have the structural character of a-SiO_2 but also contain a small proportion of critsobalite structural units; features of α quartz are not present in either SiK- or SiL-edge spectra of theses two opals. Opal no. 800 has a greater component of cristobalite structural

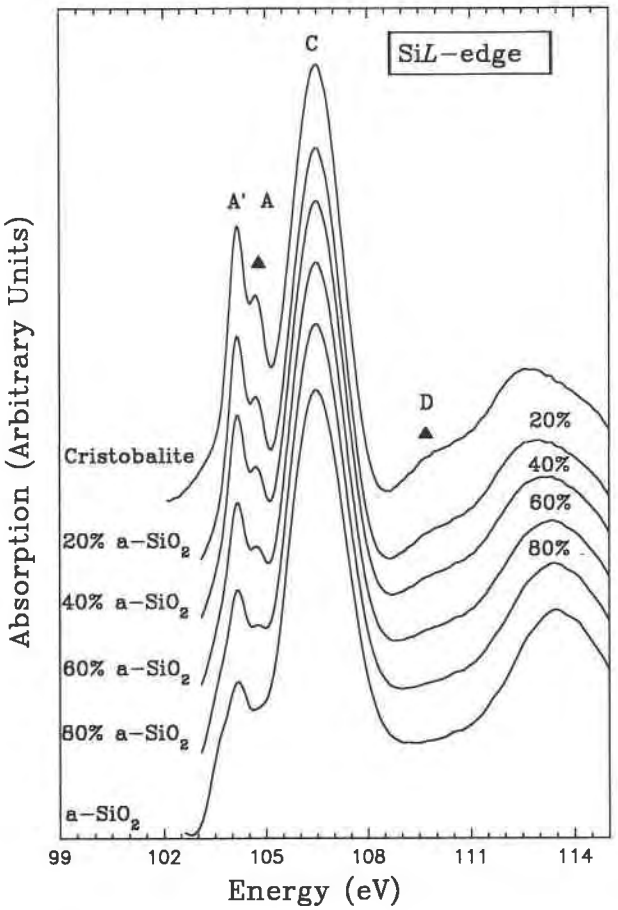

Fig. 5. SiL-edge XANES spectra of cristobalite and a-SiO_2, together with the composite spectra for various proportions of cristobalite and a-SiO_2. The spectra of cristobalite and a-SiO_2 were collected at similar experimental conditions and normalized by I/I_0. A linear background has been removed, and peak C is normalized to the same height in all these spectra. Two apparent changes, marked by solid triangles, can be observed with an increase in the proportion of cristobalite. First, peak A becomes more intense and more significantly split. Second, peak D becomes more significant.

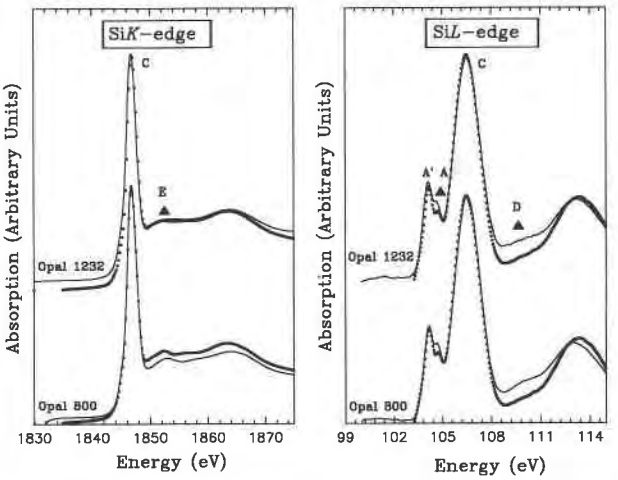

Fig. 6. **(Left)** The SiK-edge XANES spectra of two opal samples, nos. 1232 and 800, are shown (solid lines) and compared with the composite spectra (solid and dotted lines) of 10% cristobalite + 90% a-SiO_2 and 30% cristobalite + 70% a-SiO_2, respectively. **(Right)** The SiL-edge spectra of these two opals are shown (solid lines) and compared with the composite spectra of 40% cristobalite + 60% a-SiO_2 (solid and dotted lines).

units than the precious opal, no. 1232. These results are in good qualitative agreement with the X-ray diffraction patterns of the opals.

To determine the compositional and structural features of the two opals semiquantitatively, we have calculated composite SiK- and SiL-edge XANES spectra for various proportions of cristobalite and a-SiO_2, as shown in Figures 4 and 5, respectively. The SiK-edge spectra (Fig. 4) of cristobalite and a-SiO_2 were collected by TEY at similar conditions and normalized by I/I_0, where I_0 is the intensity of photon flux and I is the intensity of TEY signal. The linear background was removed, and peak C was normalized to the same height in all spectra. The most apparent feature of the composite spectra is that peak E, marked by a solid triangle in Figure 4, becomes more intense, and also peaks D and F become more significant, with an increase in the proportion of cristobalite.

Similarly, the SiL-edge spectra of cristobalite and a-SiO_2 (Fig. 5) were also collected by TEY at similar conditions and normalized by I/I_0. The linear background was subtracted, and peak C was normalized to the same height in all spectra. In the composite spectra, two apparent changes, marked by solid triangles in Figure 5, occur with an increase in the proportion of cristobalite. First, peak A becomes more intense and is split more significantly because of the spin-orbit interaction of Si 2p orbitals. Second, peak D, attributable to the MS effect of the extended structure, becomes more significant.

The SiK-edge spectra of opal nos. 1232 and 800, shown as solid lines in the left part of Figure 6, were also collected at similar experimental conditions, and the data were reduced in a similar way, as for cristobalite and a-SiO_2. Composite spectra of 10% cristobalite + 90% a-SiO_2 and 30% cristobalite + 70% a-SiO_2 simulate visually the spectra of opal nos. 1232 and 800, respectively, quite successfully. This analysis indicates that the two opal samples are essentially characterized by a-SiO_2 structural units but also contain small proportions of the structural units of crystalline cristobalite. The precious opal, no. 1232, contains about 10% cristobalite structural units, and opal no. 800 contains about 30% cristobalite structural units. These estimates are in qualitative agreement with XRD, which indicates that there is some crystalline cristobalite present. However, the XANES method can also provide information on the local structure and can semiquantitatively determine the proportions of various structural units in the opals.

The SiL-edge spectra of the two opals are shown also as

TABLE 3. EXAFS analysis of α quartz, stishovite, and amorphous SiO_2

	EXAFS analyses									X-ray diffraction	
	Rehr et al. (1991)			McKale et al. (1988)			Curve fitting				
	BD	CN	σ^2	BD	CN	σ^2	BD	CN	σ^2	BD	CN
α quartz*	1.62	3.3	0.0008	1.62	2.2	0.0003	1.61	4.6	0.002	1.61	4
Natural stishovite**	1.83	6.8	0.0040	1.77	4.5	0.0035	1.82	4.2	0.007	1.81	4
							1.77	2.2	0.007	1.76	2
Synthetic stishovite	1.86	6.6	0.0026	1.80	3.7	0.0007	1.82	3.5	0.005	1.81	4
							1.77	1.8	0.005	1.76	2
a-SiO_2†	1.61	3.4	0.0025	1.59	2.2	0.0011	1.58	1.4	0.0026		

Note: BD = bond distance (Å); CN = coordination number; σ^2 = Debye-Waller factor.
* X-ray diffraction data are cited from LePage et al. (1980).
** X-ray diffraction data are cited from Sinclair and Ringwood (1978).
† EXAFS structure parameters are derived using phase shifts and amplitudes from α quartz EXAFS analysis.

solid lines in the right part of Figure 6. Peak A is marginally stronger, and peak D is a little more significant in opal no. 800 than in opal no. 1232, qualitatively indicating that opal no. 800 has more features of crystalline cristobalite. However, these two spectra are in general very similar. The composite spectrum of 40% cristobalite + 60% a-SiO_2 fits the spectra of both opals reasonably well. Therefore, the Si*L*-edge spectra demonstrate that both opals contain about 40% cristobalite structural units and are thus in qualitative, but not quantitative, agreement with the Si*K*-edge spectra and XRD. However, as a semiquantitative method, Si*K*- and Si*L*-edge XANES shows potential applications for the characterization of the structure of opal and other partly ordered silicate materials. A more extensive range of opal samples is being investigated to determine their structure and compositions using this method. This new application of XANES to studies of amorphous and very disordered structures will be further developed in this future study.

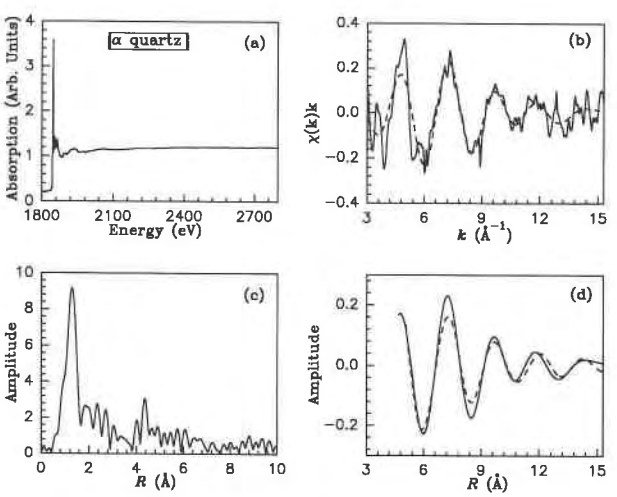

Fig. 7. The normalized Si*K*-edge EXAFS spectrum (**a**) and the data reduction of α quartz. The weighted $\chi(\mathbf{k})\cdot\mathbf{k}$ (solid lines) and the Fourier transform (dashed line) are shown in **b** and **c**, respectively. Part **d** shows the back Fourier transform (solid line) and the fitting curve (dashed line) for windowing the first shell of Si as in **c**. In part **b** the back Fourier transform for the first shell is also compared with the weighted $\chi(\mathbf{k})\cdot\mathbf{k}$.

EXAFS analysis

The application of synchrotron radiation and short-range single-electron scattering theory has made EXAFS spectroscopy a powerful technique for studying the structure of minerals and glasses (Waychunas et al., 1986). Figure 7 shows the calibrated and normalized average Si*K*-edge EXAFS spectra and EXAFS data reductions of α quartz. The EXAFS analyses were performed with the program BAN (Tyliszczak, 1992). The experimental average spectrum was normalized using I/I_0 (see Fig. 7a). Following background subtraction, the spectrum was converted from energy space into **k** space, and the weighted $\chi(\mathbf{k})\cdot\mathbf{k}$ is shown as the solid line in Figure 7b. The Fourier transform is shown in Figure 7c. Figure 7d shows the back Fourier transform (solid line) for windowing the first shell of Si in quartz, and the dashed lines are the fitting curves constructed on the basis of the above formula using theoretical amplitudes and phase shifts, as well as assumed structure parameters, bond distances, coordination numbers, and Debye-Waller factors (σ^2). Also using Rehr and McKale phase shifts and amplitude correction (Rehr et al., 1991; McKale et al., 1988), the average bond distance and coordination number for each shell were obtained. The EXAFS parameters for α quartz, stishovite, and a-SiO_2 are given in Table 3, and the bond distances and coordination numbers for α quartz and stishovite are in good agreement with the data for X-ray structures (LePage et al., 1980; Sinclair and Ringwood, 1978). The $^{[6]}$Si and $^{[4]}$Si can be determined clearly from the EXAFS analysis. In general, the bond distances derived from EXAFS are accurate to ±0.02 Å, and the coordination numbers are accurate to ±20% for the first shell.

As shown in Table 3, although the Debye-Waller factors derived using Rehr and McKale theoretical phase shifts and amplitudes and from curve fitting are different in value, the qualitative results have significance. The Debye-Waller factor, which directly measures the local vibrations of Si-O bonds, is significantly larger for stishovite than for α quartz. This is also in agreement with their structure and bonding features. For 6:3-coordinated stishovite, the Si-O bond distances are larger than those in 4:2-coordinated α quartz, and the Si-O bonds

in stishovite are of greater ionicity than they are in α quartz. Interestingly, for $^{[4]}SiO_4$, the Debye-Waller factor for a-SiO_2 is apparently larger than that for α quartz, which is consistent with the structural disorder that characterizes a-SiO_2.

Acknowledgments

We thank Lin-gun Liu, Research School of Earth Sciences, Australian National University, for the provision of the natural and synthetic stishovite samples, and we acknowledge the staff at the Synchrotron Radiation Center (SRC), the University of Wisconsin, for their technical assistance and the National Science Foundation (NSF) for the support of the SRC. This work is supported by NSERC. We appreciate the very helpful suggestions and comments from J. Stebbins and two anonymous referees.

References cited

Adams, S.J., Hawkes, G.E., and Curzon, E.H. (1991) A solid state ^{29}Si nuclear magnetic resonance study of opal and other hydrous silicas. American Mineralogist, 76, 1863–1871.

Azizan, M., Baptist, R., Brenac, A., Chauvet, G., and Nguyen Tan, T.A. (1987) Etats électroniques occupés et inoccupés de SiO_2 mesurés par photoémission directe et inverse et par émission d'X mous. Journal de Physique, 48, 81–91.

Bancroft, G.M. (1992) New developments in far UV, soft x-ray research at the Canadian Synchrotron Radiation Facility. Canadian Chemical News, 44, 15–22.

Bart, F., Jollet, F., Duraud, J.P., and Douillard, L. (1993) Electronic structure of α quartz: A XANES study of empty states. Physica Status Solidi, B176, 163–176.

Bianconi, A. (1979) Core excitons and inner well resonances in surface soft x-ray absorption (SSXA) spectra. Surface Science, 89, 41–50.

Brown, F.C., Bachrach, R.Z., and Skibowski, M. (1977) $L_{2,3}$ threshold spectra of doped silicon and silicon compounds. Physical Review, B15, 4781–4788.

Brown, I.D. (1981) The bond-valence methods: An empirical approach to chemical structure and bonding. In M. O'Keeffe and A. Navrotsky, Eds., Structure and bonding in crystals, p. 1–30. Academic, New York.

Brytov, I.A., Konashenok, K.I., and Romashchenko, Yu.N. (1979) Crystallochemical effects on Al K and Si K emission and absorption spectra for silicate and aluminosilicates. Geochemistry International, 16 (1), 142–154.

Chao, E.C.T., Fahey, J.J., Littler, J., and Milton, D.J. (1962) Stishovite, SiO_2, a very high pressure new mineral from Meteor Crater, Arizona. Journal of Geophysical Research, 67, 419–421.

Davoli, I., Paris, E., Stizza, S., Benfatto, M., Fanfoni, M., Gargano, A., Bianconi, A., and Seifert, F. (1992) Structure of densified vitreous silica: Silicon and oxygen XANES spectra and multiple scattering calculations. Physics and Chemistry of Minerals, 19, 171–175.

Dehmer, J.L. (1972) Evidence of effective potential barriers in the x-ray absorption spectra of molecules. Journal of Chemical Physics, 56, 4496–4504.

Ferrett, T.A., Lindle, D.W., Heimann, P.A., Kerkhoff, H.G., Becker, U.E., and Shirley, D.A. (1986) Sulfur 1s core-level photoionization of SF_6. Physical Review, A34, 1916–1930.

Ferrett, T.A., Piancastelli, M.N., Lindle, D.W., Heimann, P.A., and Shirley, D.A. (1988) Si 2p and 2s resonant excitation and photoionization in SiF_4. Physical Review, A38, 701–710.

Filatova, E.O., Vinogradov, A.S., and Zimkina, T.M. (1985) Fine structure of the 2p absorption spectra of silicon compounds. Soviet Physics, Solid State, 27, 606–608.

Friedrich, H., Sonntag, B., Rabe, P., Butscher, W., and Schwarz, W.H.E. (1979) Term-values and valence-Rydberg mixing in core-excited states: SiH_4 and PH_3. Chemical Physics Letters, 64, 360–366.

Hansen, P.L., Brydson, R., and McComb, D.M. (1992) p → p transitions at the silicon $L_{2,3}$-edges of silicates. Microscopy Microanalysis Microstructure, 3, 213–219.

Hill, R.J., Newton, M.D., and Gibbs, G.V. (1983) A crystal chemical study of stishovite. Journal of Solid State Chemistry, 47, 185–200.

Hudson, E., Shirley, D.A., Domke, M., Remmers, G., Puschmann, A., Mandel, T., Xue, C., and Kaindl, G. (1993) High-resolution measurements of near-edge resonances in the core-level photoionization spectra of SF_6. Physical Review, A47, 316–373.

Iguchi, Y. (1977) Soft x-ray spectra of solids containing silicon in tetrahedral and octahedral coordination with oxygen. Science of Light, 26, 161–181.

Jones, J.B., and Segnit, E.R. (1971) The nature of opal. I. Nomenclature and constituent phases. Journal of the Geological Society of Australia, 18, 57–68.

Kisiel, A., Dalba, G., Fornasini, P., Podgórny, M., Oleszkiewicz, J., Rocca, F., and Burattini, E. (1989) X-ray-absorption spectroscopy of ZnTe, CdTe, and HgTe: Experimental and theoretical study of near-edge structure. Physical Review, B39, 7895–7904.

Langer, K., and Flörke, O.W. (1974) Near infrared absorption spectra (4000–9000 cm^{-1}) of opal and the role of "water" in these $SiO_2 \cdot nH_2O$ minerals. Fortschritte der Mineralogie, 52, 17–25.

LePage, Y., Calvert, L.D., and Gabe, E.J. (1980) Parameters variation in low quartz between 94 and 298 K. Journal of Physics and the Chemistry of Solids, 41, 721–725.

Li, Dien, Bancroft, G.M., Kasrai, M., Fleet, M.E., Feng, X.H., Tan, K.H., and Yang, B.X. (1993) High-resolution Si K- and $L_{2,3}$-edge XANES of α quartz and stishovite. Solid State Communications, 87, 1613–1617.

Li, Y.P., and Ching, W.Y. (1985) Band structures of all polycrystalline forms of silicon dioxide. Physical Review, B31, 2172–2179.

Liu, L.G. (1975) Post-oxide phases of olivine and pyroxene and mineralogy of the mantle. Nature, 258, 510–512.

Liu, Z.F., Cutler, J.N., Bancroft, G.M., Tan, K.H., Cavell, R.G., and Tse, J.S. (1992) Crystal field splittings of continuum d orbitals. A comparative study on the $L_{2,3}$ edge x-ray absorption spectra of Si, P and S compounds. Chemical Physics, 168, 133–144.

McComb, D.W., Brydson, R., Hansen, P.L., and Payne, R.S. (1992) Qualitative interpretation of electron energy-loss near-edge structure in natural zircon. Journal of Physics: Condensed Matter, 4, 8363–8374.

McKale, A.G., Veal, B.W., Paulikas, A.P., Chan, S.K., and Knapp, G.S. (1988) Improved ab initio calculations of amplitude and phase functions for extended x-ray absorption fine structure spectroscopy. Journal of the American Chemical Society, 110, 3763–3768.

Natoli, C.R. (1984) Distance dependence of continuum and bound state of excitonic resonance in x-ray absorption near-edge structure (XANES). In K.O. Hodgson, B. Hedman, and J.E. Penner-Hahn, Eds., EXAFS and near-edge structure III, p. 38–42. Springer-Verlag, Berlin.

Natoli, C.R., and Benfatto, M. (1986) A unifying scheme of interpretation of x-ray absorption spectra based on the multiple scattering theory. Journal de Physique Colloque, 47, 11–24.

Nucho, R.N., and Madhukar, A. (1980) Electronic structures of SiO_2: α quartz and the influence of local disorder. Physical Review, B21, 1576–1588.

O'Brien, W.L., Jia, J., Dong, Q.Y., Callcott, T.A., Rubensson, J.E., Mueller, D.L., and Ederer, D.L. (1991) Intermediate coupling in L_2-L_3 core excitons of MgO, Al_2O_3 and SiO_2. Physical Review, B44, 1013–1018.

Okura, T., Inoue, H., Kanazawa, T., Endo, S., Fukushima, S., and Gohshi, Y. (1990) Molecular orbital calculation of Si$K\alpha$ chemical shift due to coordination in silicates and silico-phosphates. Spectrochimica Acta, B45, 711–717.

Ravindra, N.M., and Narayan, J. (1987) Optical properties of silicon related insulators. Journal of Applied Physics, 61, 2017–2021.

Rehr, J.J., de Mustre, L.J., Zabinsky, S.I., and Albers, R.C. (1991) Theoretical x-ray absorption fine structure standards. Journal of the American Chemical Society, 113, 5135–5140.

Ross, N.L., Shu, J.F., Hazen, R.M., and Gasparik, T. (1990) High-pressure crystal chemistry of stishovite. American Mineralogist, 75, 739–747.

Sinclair, W., and Ringwood, A.E. (1978) Single crystal analysis of the structure of stishovite. Nature, 272, 714–715.

Smith, J.V., and Blackwell, C.S. (1983) Nuclear magnetic resonance of silica polymorphs. Nature, 303, 223.

Stishov, S.M., and Popova, S.V. (1961) New dense polymorphic modification of silica. Geokhimiya, 10, 837–839.

Sutherland, D.G.J., Kasrai, M., Bancroft, G.M., Liu, Z.F., and Tan, K.H. (1993) Si L- and K-edge x-ray-absorption near-edge spectroscopy of gas-phase $Si(CH_3)_x(OCH_3)_{4-x}$. Physical Review B, 48, 14989–15001.

Tossell, J.A. (1975a) The electronic structures of silicon, aluminum and magnesium in tetrahedral coordination with oxygen from SCF-Xα MO calculations. Journal of the American Chemical Society, 97, 4840–4844.

——— (1975b) The electronic structures of Mg, Al and Si in octahedral coordination with oxygen from SCF Xα MO calculations. Journal of Physics and Chemistry of Solids, 36, 1273–1280.

Tse, J.S., Liu, Z.F., Bozek, J.D., and Bancroft, G.M. (1989) Multiple-scattering Xα study of the silicon and chlorine core-level photoabsorption spectra of $SiCl_4$. Physical Review, A39, 1791–1799.

Tyliszczak, T. (1992) BAN data analysis program.

Wagner, C.D., Passoja, D.E., Hillery, H.F., Kinisky, T.G., Six, H.A., Jansen, W.T., and Taylor, J.A. (1982) Auger and photoelectron line energy relationships in aluminum-oxygen and silicon-oxygen compounds. Journal of Vacuum Science and Technology, 21, 933–944.

Waychunas, G.A., Brown, G.E., Jr., and Apted, M.J. (1986) X-ray *K*-edge absorption spectra of Fe minerals and model compounds. II. EXAFS. Physics and Chemistry of Minerals, 13, 31–47.

Wiech, G., and Kurmaev, E.Z. (1985) X-ray emission bands and electronic structures of crystalline and vitreous silica (SiO_2). Journal of Physics: Solid State Physics, C18, 4393–4402.

Wong, J., and Angell, C.A. (1976) Glass structure by spectroscopy. Marcel Dekker, New York.

Yang, B.X., Middleton, F.H., Olsson, B.G., Bancroft, G.M., Chen, J.M., Sham, T.K., Tan, K.H., and Wallace, J.D. (1992) The design and performance of a soft x-ray double crystal monochromator beamline at Aladdin. Nuclear Instruments and Methods in Physics Research, A316, 422–436.

Manuscript received November 30, 1993
Manuscript accepted March 21, 1994